Superhydrophobic Stearic Acid Deposited by Dip-Coating on AISI 304 Stainless Steel: Electrochemical Behavior in a Saline Solutions

D. Guerra Sacilotto[a]* , J. Soares Costa[a], J. Zoppas Ferreira[a]

[a]Universidade Federal do Rio Grande do Sul (UFRGS), Laboratório de Corrosão, Proteção e Reciclagem (LACOR), Programa de Pós-Graduação em Engenharia de Minas, Metalúrgica e de Materiais, Porto Alegre, RS, Brasil.

A superhydrophobic surface with excellent corrosion resistance was prepared on sandblasted AISI 304 stainless steel by applying stearic acid through dip-coating. Superhydrophobic surfaces have several advantages, such as self-cleaning, anti-icing, anti-adherent, and anti-corrosion. In this work, roughness and superhydrophobic properties were studied by contact angle, optical profilometry, electrochemical impedance spectroscopy, and potentiostatic polarization techniques. The lowest surface wettability was obtained in sandblasted samples (146.2°, due to the roughness change). The stearic acid coating response on sandblasted substrates was acquired by EIS analysis. The sample set with higher corrosion resistance at saline solution during the polarized potentiostat tests was the smoothly coated sandblasted samples. For comparison, corrosion current density of sample without coating was 3.13×10^{-7}, whilst the coated sample was 1.34×10^{-8}. Further, the passive current density was 6.02×10^{-7} for as-received samples and 2.16×10^{-8} for coated samples. The modified surface proved to be effective against corrosion when compared to smooth surfaces.

Keywords: *superhydrophobic coating, stainless steel, corrosion, contact angle, stearic acid.*

1. Introduction

One of the most mimicked strategies of the leaves is the water repellency behavior, known as superhydrophobic properties[1-3]. This phenomenon can be seen in some leaves present in nature, such as Nelumbo nucifera (better known as Lotus leaf)[4], red rose petals[5], Salvinia molesta[6], and cactus spines[7]. Research on superhydrophobic surfaces has commonly received considerable attention in recent years. It can provide a passive solution to protect metal surfaces (mainly stainless steel) from various corrosion attacks in harsh environments[8,9]. Stainless steels are used in different applications owing to their mechanical and corrosion properties[10,11]. Although stainless steels generally have good corrosion resistance, they are susceptible to pitting corrosion in humid environments because of their high wettability[12]. To further increase the corrosion resistance of stainless steels, their surfaces can be modified to exhibit superhydrophobic properties (where the metal ions cannot be transported to complete the electrochemical oxidation process). Several methods have been successfully developed to manufacture and apply coatings on various substrates[3,13-15].

For a material to be considered hydrophobic, its contact angle must be greater than 90° and superhydrophobic when the angle is greater than 150°[16-18]. This behavior is governed by the surface's chemical composition and geometric structure[19,20]. Therefore, it is necessary to obtain a surface structure in micro/nanoscale and material with low surface energy. According to Wenzel[20] Cassie-Baxter models[21],

it is possible to obtain hydrophobic surfaces on smooth morphology by modifying the chemical composition and/ or modifying the surface's roughness.

The coatings/materials that have fluorocarbons in the molecular chain are the ones that have a more hydrophobic character, followed by fluorocarbons with silanes that provide greater adhesion to the substrate[22-27]. The roughness tunability is the key to controlling the contact interface, thus the wettability of the solid surface. Many methods have been developed to produce superhydrophobic surfaces, laser treatment[28,29], sol-gel[30], chemical attack[31,32], electroless deposition[33], chemical vapor deposition[34,35], template method[36,37], chemical modification[38,39], spin coating[40,41] particle coating[42] and spray coating[43,44].

Many researchers have successfully developed superhydrophobic surfaces using steel as a substrate. However, most of them have used more than one process to obtain roughness to achieve angles greater than 150°[45]. Amiriafshar et al[15]. approach included sandblasting or ground process on stainless steel surface, followed by electrodeposited zinc, before applying the stearic acid coating. In this study, the authors could not measure the contact angle of a 5μL water droplet as it drop-rolled off from the surface instantaneously. Wang et al.[46] used the stearic acid coating on stainless steel AISI 304. Two different processes were carried out before applying the coating: (i) electrocleaning; (ii) nickel plating. In the plating process, the better sample showed 158° of repellency, obtained with 16 V voltage for 5 minutes at a brush speed of 8 m/min.

---

*e-mail: daianasacilotto@gmail.com

This study aims to obtain a superhydrophobic surface using a scalable, simple, and inexpensive method aimed at industrial application. To minimize the production costs of the coating and increase the corrosion resistance of stainless steel AISI 304, this work was developed using stearic acid (SA) by dip-coating deposition method. Stearic acid is a fatty acid with 18 carbons in the molecular chain and can be easily found on the market with cheaper values than fluorinated and silanes. The roughness was obtained by the sandblasting method and the contact angle by optical profilometry equipment. Scanning electron microscope (SEM) analysis was used to evaluate the surface of the substrates at the microscale. Likewise, the corrosion behavior was evaluated by electrochemical impedance spectroscopy and potentiostatic polarization techniques.

2. Materials and Methods

2.1. Synthesis of the superhydrophobic coating

Stainless steel AISI 304 in sheet format (70 mm x 40 mm x 1mm) was used as a substrate. The sandblasting process was carried out (in some samples) to obtain the surface roughness. It was performed using the Basic Master Renfert equipment with alumina oxide particles (50 μm). Afterward, the substrates were cleaned using the commercial alkaline degreaser (Saloclean 667N). Subsequently, the samples were immersed in an ethanolic stearic acid solution, prepared using 1% stearic acid (SA - Aldrich Chemistry). The solution remained in magnetic stirring for 30 min to dissolve the granules of SA. The samples were dip-coated with an angle of 90º (Disc Lift MA 765 Marconi), remaining immersed in the solution for 3 min and the withdrawal speed was 21 cm/min. Then, the films were dried at 80°C, in a previously heated oven, for 60 min.

2.2. Characterization

Profilometry analysis was carried out to compare the roughness between the substrates (rough (R>1) and smooth (R<1) surfaces) using the 3D Bruker Optical Profilometer (GTKM, CONTOURGTK). Contact angle (CA) analyses were performed with water drops (3 μL) on the substrate, using the Drop Shape Analyzer (DSA30 - Krüss). Top-view imaging was performed by conventional scanning electron microscopy (SEM, JSM 6060 JEOL) to evaluate the aspect of the surface of the substrates at the microscale. The electrochemical experiments were conducted at room temperature in aerated 0.1 mol/L NaCl solution at pH 6. The counter-electrode used was a platinum sheet near the working electrode. The reference electrode was a silver/silver chloride saturated electrode (Ag/AgCl). The three-electrode setup was controlled by an Autolab (PGSTAT 302, Ecochemie) potentiostat, with the working electrode exposed area of 1.0 cm^2. The applied frequency domain ranged from 10^5 Hz to 10^{-2} Hz. The sinusoidal perturbation was 10 mV. The samples were monitored between 0 h to 96 h (when constantly immersed in NaCl electrolyte). In potentiostatic polarization experiments, the OCP was performed after 5 minutes to stabilize the potential after immersion of the sample in the solution. The scanning gap was -0.400 V to +0.800 V, with a scanning speed of 1 mV.s^{-1}.

3. Results and Discussion

Figure 1a and 1b shows the profilometry performed on the sample with a smooth surface, visually free of any roughness or imperfection. When analyzed more deeply, it's possible to observe the presence of roughness (red color) that is found to be heterogeneously distributed on the stainless-steel substrate (3D image - (Figure 1a). The mean arithmetic height of the smooth sample surface, Ra, is 0.19 μm while the Rq is 0.27 μm.

Observing the x and y axes, respectively, in the 2D image (Figure 1b), it is observed that the standard deviation of the height, Rq, is more accentuated in specific regions of the surface that are represented by peaks above the average height line[40].

Smooth surface

(a)

(b)

(c)

(d)
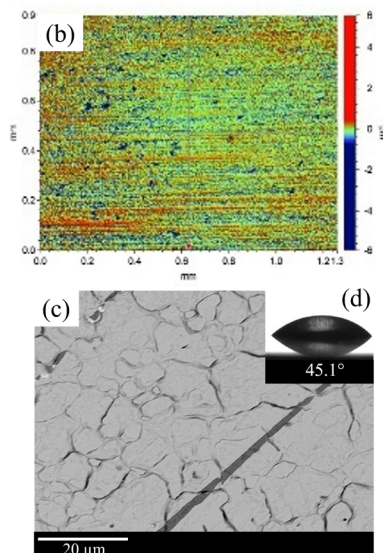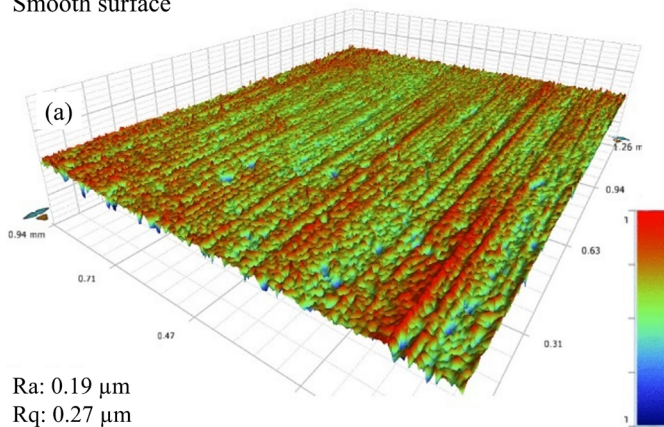
45.1°

20 μm

Ra: 0.19 μm
Rq: 0.27 μm

Figure 1. Optical profiling in 3D (a) and 2D (b), top-view SEM image (c), and a contact angle (d) of the smooth stainless-steel substrate uncoated.

Superhydrophobic Stearic Acid Deposited by Dip-Coating on AISI 304 Stainless Steel: Electrochemical
Behavior in a Saline Solutions

3

In addition, Figure 1c shows the SEM images of the smooth stainless-steel substrate uncoated with a contact angle of 45.1° (Figure 1d). It is possible to verify the grain boundary and the presence of scratches on the surface of the substrate. The scratches present on the surface, when deep, can act as places to increase wettability, trapping small particles of water or electrolyte solutions, which can trigger corrosive processes.

The roughness obtained through the sandblasting process, Figure 2a-d, shows the roughness Ra of 1.81 μm, being defined as a rough surface because it has a Ra value greater than 1 μm.

When verifying the 3D image (Figure 2a), the distribution of peaks is observed throughout the analyzed area. However, when checking the 2D image (Figure 2b), x and y axes, it is verified that the distribution of peaks and valleys and the height are not standardized. This variation can influence the surface's wettability after coating, making points more or less hydrophobic. The wide variation between valleys and peaks represents the Rq of 2.48 μm[27].

Furthermore, Figure 2c shows the SEM images of the sandblasted stainless-steel substrate uncoated with a contact angle of 24.4° Figure 2d). The increase in wettability, that is, the smaller contact angle is due to the rise in the surface area provided by the roughness. This scattering of the water droplet, greater than the sample with the smooth surface, the blasted surface becomes chemically more active, causing the cohesive forces of the molecules of the water droplet to become weaker than the surface energy acting on the water droplet therefore present greater scattering over the metallic surface. It is possible to ascertain that the sample has a heterogeneous rough morphology at the smaller contact angle. It is impossible to detect the presence of valleys and peaks accurately, as can be seen through profilometry (Figure 2a, 2b).

In Figure 3, it is possible to observe the top-view SEM micrographs and the contact angle of the stainless-steel substrate with a smooth (a) and sandblasted surface (b) with a stearic acid (SA) coating.

It is possible to check the grain boundaries on the stainless-steel surface using conventional SEM. When comparing the surface of the sample coated with stearic acid in Figure 3a with Figure 1c, it is possible to note the presence of small white dots (indicated by arrows) on the coated surface. Sandblasted surfaces with a stearic acid coating (Figure 3b) present a heterogeneous rough structure when analyzed at 20μm. However, the morphology is homogeneous when verifying the structures in different magnification scales (200μm - not shown here). The presence of irregular dots (at a small scale) is prone to liquids adherence, defined as a petal effect. This effect occurs due to the structural variation in smaller scales inducing the aqueous particles imprisonment due to the increased wettability and presented roughness. Likewise, the samples with SA coating showed contact angles of 114.2 ° for the smooth surface (Figure 3a) and 146.2 ° for the sandblasted surface (Figure 3b). The presence of the SA coating increased the hydrophobicity of the sample with a smooth surface by 69.1 ° and 121.8 ° for the rough surface (not shown here). The sandblasted surface presents a relevant gap in wettability when the coating is present. This considerable change happens because the sandblasted uncoated sample has a greater surface area, provided by the peaks and valleys. This surface shape favors the penetration of water between the cavities, increasing the spread of the drop over the surface[47]. Physically explaining, the cohesive forces of the water molecule present a force smaller than the adhesion force that the metallic surface exerts on the water drop. In this way, the drop ends up spreading and presenting greater wettability on the rough surface when compared to the smooth surface, both without coating. The adhesion force is higher on the sandblasted surface because the atoms on the surface area are chemically more active, due to the lack of neighboring atoms to share the charges. Also, the smooth
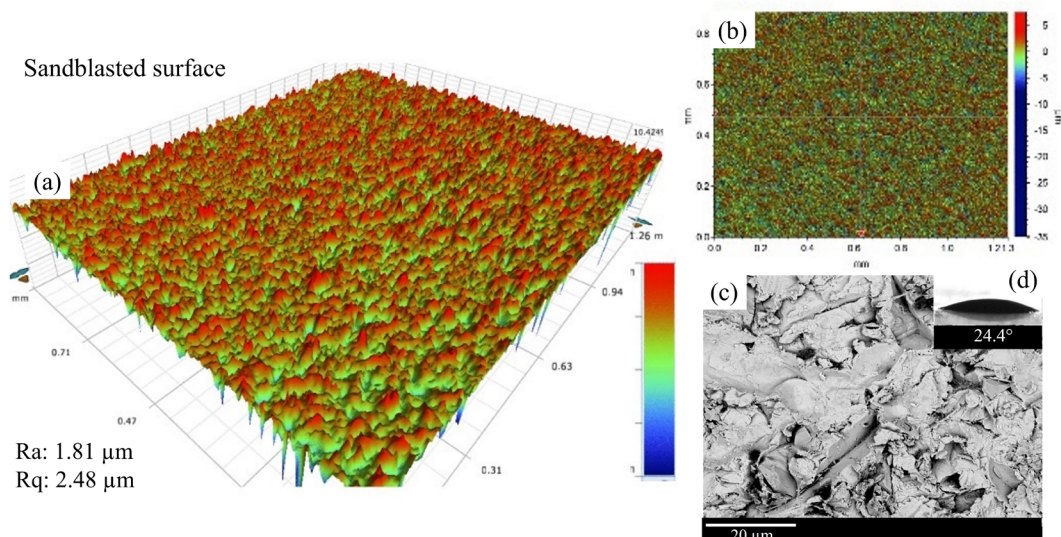

Figure 2. Optical profiling in 3D (a) and 2D (b), top-view SEM images (c), and a contact angle (d) of the sandblasted stainless-steel substrate uncoated.
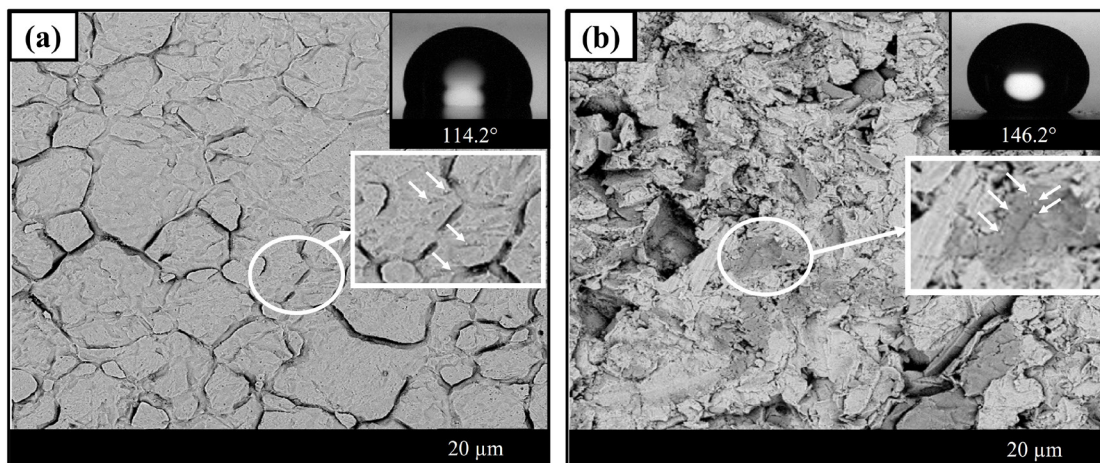
Figure 3. Top-view SEM micrographs and contact angle of the stainless-steel substrate with a smooth (a) and sandblasted surface (b) with a stearic acid (SA) coating.

surface has fewer active atoms present on the surface due to the soft structure that this surface shows[48].

It is observed that the blasted surface, combined with the low free energy surface coating, practically doubled the value of the increase in hydrophobicity in relation to the smooth substrate[49,50]. In other words, when the arithmetic roughness (Ra) of the surface is considered a smooth surface, that is, Ra <1, the Cassie-Baxter theory is not applied. However, for sandblasted surfaces (Ra > 1), the contact angle can exceed 150°, making it a superhydrophobic surface[19,50,51].

To evaluate the durability and corrosion protection provided by the stearic acid coating, electrochemical impedance spectroscopy was realized in 0.1 mol/L NaCl solution. Figure 4 shows the Nyquist diagram in 48 h of immersion in NaCl solution. All the samples show only one capacitive arc with a different radius, where, generally, the larger arc corresponds to the better corrosion resistance[52]. The behavior verified at high frequency is attributed to the solution resistance[53].

After 48 h of immersion in the solution, the hydrophobic coatings' capacitive loop continues better than the bare sample. This indicates that the stearic acid coating shows good protection in a corrosive environment, as indicated in low-frequency behavior[54]. Among the coated samples, the sample with a smooth surface has higher impedance when compared to the sandblasted surface. Although the sandblasted/SA showed lower wettability, the soft/SA sample has a stable chromium oxide layer, which was removed from the sandblasted/SA sample when performing the sandblasting process.

According to the authors[15], the sandblasted and ground surfaces have uncoated regions, exposing these areas to the electrolytic solution. These surfaces, with the highest and lowest roughness and poor coating quality, show more reduction in the contact angles when compared with the as-received coated samples. It also mentions that the as-received selection has excellent uniformity and adhesion durability of the coating when compared to samples with modified surface roughness.

To investigate the corrosion resistance of the hydrophobic coating, the electrochemical impedance spectroscopy was realized until 96 h. Figure 5 shows the behavior of the samples
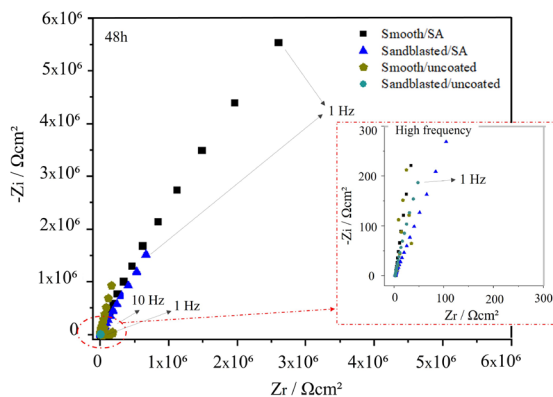

Figure 4. Nyquist diagram for smooth and sandblasted substrates with SA coating compared to the uncoated substrates, analyzed in 48 h of immersion in 0.1 mol / L NaCl solution.

in 30 min, 48 h, and 96 h of immersion in electrolyte solution through the Bode diagrams.

After 0.5h of immersion time, the smooth/uncoated sample shows the impedance modulus (|Z|) close to 1 Ωcm^2 in low frequency, and the corresponding phase angle is close to -80. Comparing the uncoated surfaces, the sandblasted surface has low corrosion resistance when compared to the smooth surface, the impedance modulus is next to 0.01 Ωcm^2 and the phase angle is close to -60. This behavior indicates that the morphological features of the blasting process, together with the modification of the chromium oxide layer, makes the surface more susceptible to electrolytic attack. When analyzing the Smooth/SA substrate, the impedance modulus is near 10 Ωcm^2, and the phase angle is close to -60. Similar behavior can also be verified for the sandblasted/SA substrate. Still, the impedance modulus shows an intermediate value to the samples with smooth SA coating and bare surface in low frequency. Some authors[55] reported similar results using titanium dioxide-fluorosiloxane superhydrophobic coating on stainless steel AISI 304.
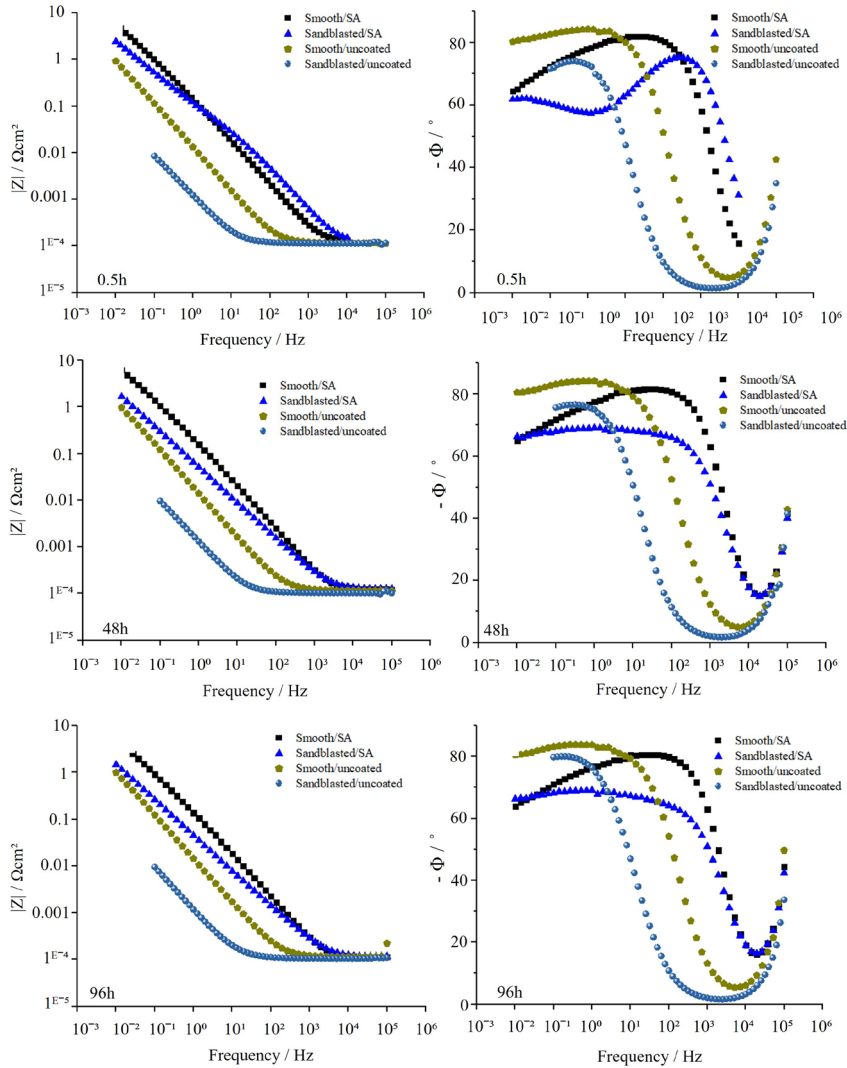
Figure 5. Bode diagrams of the samples with the smooth and sandblasted substrate with SA coating compared to the uncoated substrates analyzed in 0.5 h, 48 h, and 96 h of immersion in 0.1 mol / L NaCl solution.

From the phase diagram we observed that the 0.5h immersion in NaCl solution displayed two constants for the Sandblasted/SA sample at 1Hz to 1kHz. On the other hand, the high-frequency behavior was possibly attributed to the dielectric passive film nature, which means the oxide film's resistance opposite the permeability of ions (Cl⁻)[56]. For the low frequency shows a charge transfer is happening, possible between the electrolyte and hydrophobic surface. After immersion of 48 and 96h the behavior observed at low-frequency is attributed to the double-layer capacitance due to the approximation of counter ions formed on the interfacing electrode, that get through the electrolyte and balance the charge on the electrode interface already modified with a hydrophobic coating interface. The Smooth/SA substrate exhibited better corrosion resistance than the other samples, and this behavior remains steady after 96h of immersion in the working electrolyte. It is known that smooth surfaces contribute to the uniformity and

thickness of the stearic acid coating, furthering the stable oxide layer[57]. However, as the immersion time increases, the impedance modulus becomes smaller, indicating that the corrosion resistance of hydrophobic coating gradually decreases[55]. For Smooth/uncoated substrate, only one time constant could be detected corresponding to the barrier of the passive film on the stainless steel[52].

The sandblasted substrate coated with stearic acid achieved a higher CA value because the water drop becomes in contact with air and roughness peaks (Cassie-Baxter model); nevertheless, when some regions are uncoated, the Cl⁻ ions tend to penetrate through the coating and enter in contact with the metal substrate. When the sample is immersed in the solution, and the surfaces are covered, an effective protective barrier is formed between the chloride and the sample surface. However, the smooth/SA substrate with the hydrophobic coating is effectively protected under these circumstances.

Corrosion resistance was also investigated through potentiostatic polarization, as shown in Figure 6 and Table 1, with soaking for 5 minutes, comparing the samples with and without coating through the passive current density (Ipass), corrosion current density (Icorr) and the corrosion potential (Ecorr). Generally, higher corrosion potentials (Ecorr) and lower corrosion current densities (Icorr) indicate better corrosion resistance. In addition, the polarization curves show that the hydrophobic coated samples have a left shift in the x-axis, indicating a lower corrosion current density[58]. This behavior demonstrates that the corrosion resistance has been thoroughly improved after fabricating the stearic acid-based coating layer on the stainless-steel substrate.

Table 1 shows the relationship between the water contact angle and the passive current density (Ipass). See the samples with lower wettability present the best Ipass results. In order, Sandblasted/SA gives the best result when compared to Smooth/SA (not too far), followed by the smooth and sandblasted uncoated samples, respectively. This behavior indicates that the sample with a lower passive current density (Ipass) presents greater resistance to the propagation of pits, therefore the hydrophobic coating does an important function in the protection of these substrates in a saline environment. The sandblasted/SA surface presented with the higher Ecorr -0.018 V (but not too far from the other samples) and one of
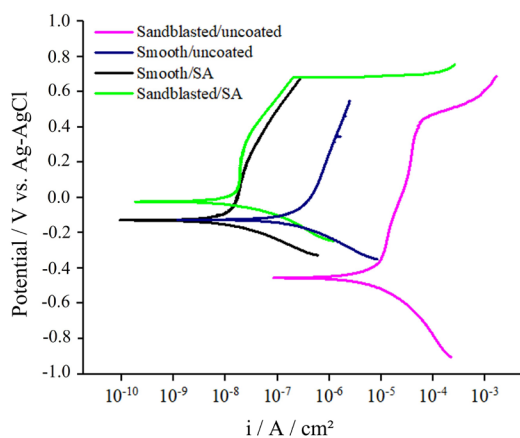
the lowest current densities (1.51×10^{-8} A.cm^{-2}). The positive potential (Ecorr) possibly indicates that the sample is more noble where an electrochemical cell occurs. The Smooth/SA sample showed good performance due to the combination of coating and the chromium oxide layer present on the surface exhibiting corrosion potential of -0.126 V and Icorr of 1.34×10^{-8} A.cm^{-2}. The increase in wettability increases the ability to propagate corrosive processes. The heterogeneity of rough surfaces can increase or decrease the hydrophobicity at a given point in the sample[59,60]. These theories can be verified through the different behavior presented by the samples with the smooth and sandblasted surface, through the EIS analysis, and potentiostatic polarization. The Icorr of the bare substrate is 3.13×10^{7} A.cm^{-2} to smooth surface and 8.05×10^{-6} A.cm^{-2} to sandblasted sample. These differences prove the strength of chromium oxide on the smooth surface and the high surface free energy on the blasted surface that is caused by the removal of chromium oxide layer together with the blasting characteristics. At the same time of the study, the anodic current densities of the SA coated steel are one magnitude order lower than the uncoated steel[55].

These results indicate that the corrosion current density of coated samples is more protective than the uncoated substrate, close to an order of magnitude. Only the sample with the sandblasted surface showed pitting potential near to 0.5 V. Is important to remember that the modification of the chromium oxide layer associated with the heterogeneity of the surface roughness and/or coating deposition (thickness), becomes prone to points for the development of pitting[55,56,61].

4. Conclusions

This paper successfully manufactures superhydrophobic coating on stainless steel AISI 304 substrates by combining the sandblasting process to surface roughness modification and the stearic acid coating. The homogeneity of the surface roughness is a determining factor in the wettability and quality of the layer. The influence of the rough surface can be verified through the contact angle, where the sandblasted/SA sample showed 146.2° while the smooth/SA sample showed 114.2°. The coated samples accomplish better results when compared to the soft/uncoated sample, proofing that the hydrophobic coating offers excellent corrosion resistance. Furthermore, the stearic acid coating applied on the smooth sample (smooth/SA) exhibits good chemical stability in the NaCl solution (results provided by EIS analysis). The methodology used in this work is effortless, effective, inexpensive, and scalable for industrial applications.

5. Acknowledgments

6. References

1. Liu K, Jiang L. Metallic surfaces with special wettability. Nanoscale. 2011;3(3):825. http://dx.doi.org/10.1039/c0nr00642d.
2. Rezayi T, Entezari MH. Fabrication of superhydrophobic iron with anti-corrosion property by ultrasound. Surf Coat Tech. 2017;309:795-804. http://dx.doi.org/10.1016/j.surfcoat.2016.10.083.

Figure 6. Polarization Curves of samples with smooth and sandblasted surface coated with SA compared with the uncoated samples analyzed in 0.1 mol / L of NaCl solution.

Table 1. Samples with water contact angle, passive current density (Ipass) corrosion current density (Icorr) and corrosion potential (Ecorr) data from the Tafel line.

Samples	Ipass (A/cm²)	Icorr (A/cm²)	Ecorr (V)
Sandblasted Uncoated (24.4°)	1.50×10^{-5}	8.05×10^{-6}	-0,450
Smooth Uncoated (45.1°)	6.02×10^{-7}	3.13×10^{-7}	-0.122
Smooth/SA (114.2°)	2.80×10^{-8}	1.34×10^{-8}	-0.126
Sandblasted/SA (146.2°)	2.16×10^{-8}	1.51×10^{-8}	-0.018

Superhydrophobic Stearic Acid Deposited by Dip-Coating on AISI 304 Stainless Steel: Electrochemical
Behavior in a Saline Solutions

7

3. Zhang C, Kalulu M, Sun S, Jiang P, Zhou X, Wei Y, et al. Environmentally safe, durable and transparent superhydrophobic coating prepared by one-step spraying. Colloids Surf A Physicochem Eng Asp. 2019;570:147-55. http://dx.doi.org/10.1016/j.colsurfa.2019.03.015.

4. Koch K, Bhushan B, Barthlott W. Multifunctional surface structures of plants: an inspiration for biomimetics. Prog Mater Sci. 2009;54(2):137-78. http://dx.doi.org/10.1016/j.pmatsci.2008.07.003.

5. Feng L, Zhang Y, Xi J, Zhu Y, Wang N, Xia F, et al. Petal effect: a superhydrophobic state with high adhesive force. Langmuir. 2008;24(8):4114-9. http://dx.doi.org/10.1021/la703821h.

6. Darmanin T, Guittard F. Superhydrophobic and superoleophobic properties in nature. Mater Today. 2015;18(5):273-85. http://dx.doi.org/10.1016/j.mattod.2015.01.001.

7. Ju J, Bai H, Zheng Y, Zhao T, Fang R, Jiang L. A multi-structural and multi-functional integrated fog collection system in cactus. Nat Commun. 2012;3(1):1247. http://dx.doi.org/10.1038/ncomms2253.

8. Meuler AJ, McKinley GH, Cohen RE. Exploiting topographical texture to impart icephobicity. ACS Nano. 2010;4(12):7048-52. http://dx.doi.org/10.1021/nn103214q.

9. Kreder MJ, Alvarenga J, Kim P, Aizenberg J. Design of anti-icing surfaces: smooth, textured or slippery. Nat Rev Mater. 2016;1(1):15003. http://dx.doi.org/10.1038/natrevmats.2015.3.

10. Lee C, Kim A, Kim J. Electrochemically etched porous stainless steel for enhanced oil retention. Surf Coat Tech. 2015;264:127-31. http://dx.doi.org/10.1016/j.surfcoat.2015.01.004.

11. Aparicio M, Jitianu A, Rodriguez G, Degnah A, Al-Marzoki K, Mosa J, et al. Corrosion protection of AISI 304 stainless steel with melting gel coatings. Electrochim Acta. 2016;202:325-32. http://dx.doi.org/10.1016/j.electacta.2015.12.142.

12. Pardo A, Merino MC, Coy AE, Viejo F, Arrabal R, Matykina E. Pitting corrosion behaviour of austenitic stainless steels – combining effects of Mn and Mo additions. Corros Sci. 2008;50(6):1796-806. http://dx.doi.org/10.1016/j.corsci.2008.04.005.

13. Zhang Q, Zhang H. Corrosion resistance and mechanism of micro-nano structure super-hydrophobic surface prepared by laser etching combined with coating process. Anti-Corros Methods Mater. 2019;66(3):264-73. http://dx.doi.org/10.1108/ACMM-07-2018-1964.

14. Yu L, Chen GY, Xu H, Liu X. Substrate-independent, transparent oil-repellent coatings with self-healing and persistent easy-sliding oil repellency. ACS Nano. 2016;10(1):1076-85. http://dx.doi.org/10.1021/acsnano.5b06404.

15. Amiriafshar M, Rafieazad M, Duan X, Nasiri A. Fabrication and coating adhesion study of superhydrophobic stainless steel surfaces: the effect of substrate surface roughness. Surf Interfaces. 2020;20:100526. http://dx.doi.org/10.1016/j.surfin.2020.100526.

16. Bonugli LO, Puydinger dos Santos MV, de Souza EF, Teschke O. Superhydrophobic polyethylcyanoacrylate coatings. Contact area with water measured by Raman spectral images, contact angle and Cassie–Baxter model. J Colloid Interface Sci. 2012;388(1):306-12. http://dx.doi.org/10.1016/j.jcis.2012.08.055.

17. Barati Darband G, Aliofkhazraei M, Khorsand S, Sokhanvar S, Kaboli A. Science and engineering of superhydrophobic surfaces: review of corrosion resistance, chemical and mechanical stability. Arab J Chem. 2020;13(1):1763-802. http://dx.doi.org/10.1016/j.arabjc.2018.01.013.

18. Bhushan B, Chae Jung Y. Wetting study of patterned surfaces for superhydrophobicity. Ultramicroscopy. 2007;107(10-11):1033-41. http://dx.doi.org/10.1016/j.ultramic.2007.05.002.

19. Lafuma A, Quéré D. Superhydrophobic states. Nat Mater. 2003;2(7):457-60. http://dx.doi.org/10.1038/nmat924.

20. Wenzel RN. Resistance of solid surfaces to wetting by water. Ind Eng Chem. 1936;28(8):988-94. http://dx.doi.org/10.1021/ie50320a024.

21. Cassie ABD, Baxter S. Wettability of porous surfaces. Trans Faraday Soc. 1944;40:546-51. http://dx.doi.org/10.1039/tf9444000546.

22. Ambrosia MS, Ha MY. A molecular dynamics study of Wenzel state water droplets on anisotropic surfaces. Comput Fluids. 2018;163:1-6. http://dx.doi.org/10.1016/j.compfluid.2017.12.013.

23. Arukalam IO, Meng M, Xiao H, Ma Y, Oguzie EE, Li Y. Effect of perfluorodecyltrichlorosilane on the surface properties and anti-corrosion behavior of poly(dimethylsiloxane)-ZnO coatings. Appl Surf Sci. 2018;433:1113-27. http://dx.doi.org/10.1016/j.apsusc.2017.10.096.

24. Alonso Frank M, Boccaccini AR, Virtanen S. A facile and scalable method to produce superhydrophic stainless steel surface. Appl Surf Sci. 2014;311:753-7. http://dx.doi.org/10.1016/j.apsusc.2014.05.152.

25. Nakajima A, Nakagawa Y, Furuta T, Sakai M, Isobe T, Matsushita S. Sliding of water droplets on smooth hydrophobic silane coatings with regular triangle hydrophilic regions. Langmuir. 2013;29(29):9269-75. http://dx.doi.org/10.1021/la401517v.

26. Nakajima A, Miyamoto T, Sakai M, Isobe T, Matsushita S. Comparative study of the impact and sliding behavior of water droplets on two different hydrophobic silane coatings. Appl Surf Sci. 2014;292:990-6. http://dx.doi.org/10.1016/j.apsusc.2013.12.097.

27. Miwa M, Nakajima A, Fujishima A, Hashimoto K, Watanabe T. Effects of the surface roughness on sliding angles of water droplets on superhydrophobic surfaces. Langmuir. 2000;16(13):5754-60. http://dx.doi.org/10.1021/la991660o.

28. Boujelbene M. Influence of the CO_2 laser cutting process parameters on the Quadratic Mean Roughness Rq of the low carbon steel. Procedia Manufacturing. 2018;20:259-64. http://dx.doi.org/10.1016/j.promfg.2018.02.038.

29. Du Q, Ai J, Qin Z, Liu J, Zeng X. Fabrication of superhydrophobic/superhydrophilic patterns on polyimide surface by ultraviolet laser direct texturing. J Mater Process Technol. 2018;251:188-96. http://dx.doi.org/10.1016/j.jmatprotec.2017.08.034.

30. Kunst SR, Cardoso HRP, Beltrami LVR, Oliveira CT, Menezes TL, Ferreira JZ, et al. New sol-gel formulations to increase the barrier effect of a protective coating against the corrosion and wear of galvanized steel. Mater Res. 2015;18(1):138-50. http://dx.doi.org/10.1590/1516-1439.288914.

31. Huang Y, Sarkar DK, Grant Chen X. Superhydrophobic aluminum alloy surfaces prepared by chemical etching process and their corrosion resistance properties. Appl Surf Sci. 2015;356:1012-24. http://dx.doi.org/10.1016/j.apsusc.2015.08.166.

32. Jie H, Xu Q, Wei L, Min Y. Etching and heating treatment combined approach for superhydrophobic surface on brass substrates and the consequent corrosion resistance. Corros Sci. 2016;102:251-8. http://dx.doi.org/10.1016/j.corsci.2015.10.013.

33. Nguyen TPN, Dufour R, Thomy V, Senez V, Boukherroub R, Coffinier Y. Fabrication of superhydrophobic and highly oleophobic silicon-based surfaces via electroless etching method. Appl Surf Sci. 2014;295:38-43. http://dx.doi.org/10.1016/j.apsusc.2013.12.166.

34. Jena G, Thinaharan C, George RP, Philip J. Robust nickel-reduced graphene oxide-myristic acid superhydrophobic coating on carbon steel using electrochemical codeposition: effect of deposition current density and electrolyte temperature on superhydrophobicity and corrosion resistance. Surf Coat Tech. 2020;397:125942. http://dx.doi.org/10.1016/j.surfcoat.2020.125942.

35. Deepa PN, Kanungo M, Claycomb G, Sherwood PMA, Collinson MM. Electrochemically deposited sol-gel-derived silicate films as a viable alternative in thin-film design. Anal Chem. 2003;75(20):5399-405. http://dx.doi.org/10.1021/ac026459o.

36. Qing Y, Long C, An K, Hu C, Liu C. Sandpaper as template for a robust superhydrophobic surface with self-cleaning and anti-snow/icing performances. J Colloid Interface Sci. 2019;548:224-32. http://dx.doi.org/10.1016/j.jcis.2019.04.040.

37. Zhang F, Shi Z, Chen L, Jiang Y, Xu C, Wu Z, et al. Porous superhydrophobic and superoleophilic surfaces prepared by template assisted chemical vapor deposition. Surf Coat Tech. 2017;315:385-90. http://dx.doi.org/10.1016/j.surfcoat.2017.02.058.

38. Hu Z, Zen X, Gong J, Deng Y. Water resistance improvement of paper by superhydrophobic modification with microsized $CaCO_3$ and fatty acid coating. Colloids Surf A Physicochem Eng Asp. 2009;351(1-3):65-70. http://dx.doi.org/10.1016/j.colsurfa.2009.09.036.

39. Ji W-G, Hu J-M, Liu L, Zhang J-Q, Cao C-N. Improving the corrosion performance of epoxy coatings by chemical modification with silane monomers. Surf Coat Tech. 2007;201(8):4789-95. http://dx.doi.org/10.1016/j.surfcoat.2006.09.100.

40. Kosak Söz C, Yilgör E, Yilgör I. Influence of the average surface roughness on the formation of superhydrophobic polymer surfaces through spin-coating with hydrophobic fumed silica. Polymer. 2015;62:118-28. http://dx.doi.org/10.1016/j.polymer.2015.02.032.

41. Navarro FH, Gómez JE, Espinal JH, Sandoval JE. Neutral hydrophilic coatings for capillary electrophoresis prepared by controlled radical polymerization. Anal Chim Acta. 2016;948:104-12. http://dx.doi.org/10.1016/j.aca.2016.10.023.

42. Aziz H, Tafreshi HV. Role of particles spatial distribution in drag reduction performance of superhydrophobic granular coatings. Int J Multiph Flow. 2018;98:128-38. http://dx.doi.org/10.1016/j.ijmultiphaseflow.2017.09.006.

43. Celik N, Torun I, Ruzi M, Esidir A, Onses MS. Fabrication of robust superhydrophobic surfaces by one-step spray coating: evaporation driven self-assembly of wax and nanoparticles into hierarchical structures. Chem Eng J. 2020;396:125230. http://dx.doi.org/10.1016/j.cej.2020.125230.

44. Feng K, Hung G-Y, Liu J, Li M, Zhou C, Liu M. Fabrication of high performance superhydrophobic coatings by spray-coating of polysiloxane modified halloysite nanotubes. Chem Eng J. 2018;331:744-54. http://dx.doi.org/10.1016/j.cej.2017.09.023.

45. Fihri A, Bovero E, Al-Shahrani A, Al-Ghamdi A, Alabedi G. Recent progress in superhydrophobic coatings used for steel protection: a review. Colloids Surf A Physicochem Eng Asp. 2017;520:378-90. http://dx.doi.org/10.1016/j.colsurfa.2016.12.057.

46. Wang L, Xing Y, Liu X, Zheng H, Song J. Fabrication of superhydrophobic surfaces on stainless steel mesh substrates via electro-brush flow plating technology. Procedia CIRP. 2018;68:232-6. http://dx.doi.org/10.1016/j.procir.2017.12.054.

47. Cabezudo N, Sun J, Andi B, Ding F, Wang D, Chang W, et al. Enhancement of surface wettability via micro- and nanostrucutres by single point Diamond turning. Nanotechnology and Precision Engineering. 2019;2(1):8-14. http://dx.doi.org/10.1016/j.npe.2019.03.008.

48. Ngo CV, Chun DM. Fast wettability transition from hydrophilic to superhydrophobic laser-textured stainless steel surfaces under low-temperature annealing. Appl Surf Sci. 2017;409:232-40. http://dx.doi.org/10.1016/j.apsusc.2017.03.038.

49. Kumar N, Wang L, Siretanu I, Duits M, Mugele F. Salt dependent stability of stearic acid Langmuir-Blodgett films exposed to aqueous electrolytes. Langmuir. 2013;29(17):5150-9. http://dx.doi.org/10.1021/la400615j.

50. David R, Neumann AW. Energy barriers between the Cassie and Wenzel states on random, superhydrophobic surfaces. Colloids Surf A Physicochem Eng Asp. 2013;425:51-8. http://dx.doi.org/10.1016/j.colsurfa.2013.02.049.

51. Kota AK, Mabry JM, Tuteja A. Superoleophobic surfaces: design criteria and recent studies. Surf Innov. 2013;1(2):71-83. http://dx.doi.org/10.1680/si.12.00017.

52. Wang Z, Shen L, Jiang W, Fan M, Liu D, Zhao J. Superhydrophobic nickel coatings fabricated by scanning electrodeposition on stainless steel formed by selective laser melting. Surf Coat Tech. 2019;377:124886. http://dx.doi.org/10.1016/j.surfcoat.2019.08.015.

53. Žerjav G, Milošev I. Protection of copper against corrosion in simulated urban rain by the combined action of benzotriazole, 2-mercaptobenzimidazole and stearic acid. Corros Sci. 2015;98:180-91. http://dx.doi.org/10.1016/j.corsci.2015.05.023.

54. Lu Y, Guan Y, Li Y, Yang L, Wang M, Wang Y. Nanosecond laser fabrication of superhydrophobic surface on 316L stainless steel and corrosion protection application. Colloids Surf A Physicochem Eng Asp. 2020;604:125259. http://dx.doi.org/10.1016/j.colsurfa.2020.125259.

55. Tan Q, Gao Z, Yan J, Xia D, Hu W. Effect of chloride ions in acid and salt solutions on self-repairing ability and corrosion performance of titanium dioxide-fluorosiloxane superhydrophobic coating. Prog Org Coat. 2020;146:105675. http://dx.doi.org/10.1016/j.porgcoat.2020.105675.

56. Hashemzadeh M, Raeissi K, Ashrafizadeh F, Khorsand S. Effect of ammonium chloride on microstructure, super-hydrophobicity and corrosion resistance of nickel coatings. Surf Coat Tech. 2015;283:318-28. http://dx.doi.org/10.1016/j.surfcoat.2015.11.008.

57. Kuang J, Ba Z, Li Z, Wang Z, Qiu J. The study on corrosion resistance of superhydrophobic coatings on magnesium. Appl Surf Sci. 2020;501:144137. http://dx.doi.org/10.1016/j.apsusc.2019.144137.

58. Wang M, Zhang D, Yang Z, Yang C, Tian Y, Liu X. A contrastive investigation on the anticorrosive performance of stearic acid and fluoroalkylsilane-modified superhydrophobic surface in salt, alkali, and acid solution. Langmuir. 2020;36(34):10279-92. http://dx.doi.org/10.1021/acs.langmuir.0c02080.

59. Rafieazad M, Jaffer JA, Cui C, Duan X, Nasiri A. Nanosecond laser fabrication of hydrophobic stainless steel surfaces: the impact on microstructure and corrosion resistance. Materails. 2018;11(9):1577. http://dx.doi.org/10.3390/ma11091577.

60. Amiriafshar M, Duan X, Nasiri A. Fabrication and corrosion performance of a superhydrophobic stainless steel surface. In: 17th International Conference Nanochannels, Microchannels, Minichannels (ICNMM 2019); 2019; St. John's, NL, Canada. Proceedings. New York: ASME; 2019. http://dx.doi.org/10.1115/ICNMM2019-4209.

61. Gadelmawla ES, Koura MM, Maksoud TMA, Elewa IM, Soliman HH. Roughness parameters. J Mater Process Technol. 2002;123(1):133-45. http://dx.doi.org/10.1016/S0924-0136(02)00060-2.